Chinese Pangolin Algorithm with a Probability-Oscillating Convergence Factor for Solving Economic Load Dispatch Problems

Hao-Ming Song, Jie-Sheng Wang*, Xin-Yi Guan, Jia-Hui Zhao

Abstract—**Economic Load Dispatch (ELD) is a core problem in power system optimization, aiming to allocate generator outputs optimally while minimizing fuel costs and power losses under system constraints and power demand requirements. To address the optimization challenges of ELD, this paper proposes an improved Chinese Pangolin Optimizer(ICPO) incorporating a probability-oscillating convergence factor strategy. This strategy integrates six different probability distributions-uniform, Beta, exponential, normal, Rayleigh, and Wei bull-to enhance the algorithm's global exploration and local exploitation capabilities, thereby improving convergence accuracy and stability. In the experimental evaluation, the performance of the improved algorithm is first validated using the CEC-BC-2022 benchmark test functions, from which the most effective strategy is selected for solving the ELD problem. The algorithm's optimization effectiveness is assessed under two typical scenarios: a 40-unit system with a load demand of 10,500 MW and a 110-unit system with a load demand of 15,000 MW. Experimental results demonstrate that the improved CPO exhibits superior convergence performance and optimization capability in handling ELD problems, providing an efficient solution for economic power system dispatch.**

Index Terms—**Economic Load Dispatch, Chinese Pangolin Optimizer, Probability-Oscillating Convergence Factor, Function Optimization**

I. Introduction

Economic Load Dispatch (ELD) is a fundamental problem in power system optimization and scheduling. Its primary objective is to optimize the power output allocation of generating units while minimizing fuel costs and power losses, ensuring system stability and reliability under system constraints and power demand requirements [1]. The ELD problem typically involves complex nonlinear constraints, including generator physical characteristics, power balance constraints, environmental factors, and other operational limitations, making its solution process highly challenging. Therefore, developing efficient, stable, and robust optimization algorithms to solve the ELD problem has become a crucial research direction in power system optimization. Traditional mathematical optimization approaches, such as linear programming, dynamic programming and Lagrangian relaxation, have demonstrated strong convergence properties and high precision when applied to small-scale, linear, or convex Economic Load Dispatch (ELD) problems. These methods efficiently determine optimal power distribution by leveraging well-established mathematical principles. However, in large-scale, highly nonlinear, and constraint-intensive power dispatch scenarios, these techniques encounter significant challenges, including excessive computational overhead, susceptibility to premature convergence at local optima, and slow convergence rates, particularly when handling complex objective functions and practical operational constraints [2].

To overcome these limitations, swarm intelligence (SI)-based meta-heuristic algorithms have gained widespread attention due to their superior global search capability, robustness, and adaptability to intricate constraints [3]. These bio-inspired methods leverage cooperative behavior and distributed problem-solving mechanisms to balance exploration and exploitation, thereby improving convergence speed and solution accuracy. Representative approaches include Particle Swarm Optimization (PSO), Genetic Algorithm (GA), and Differential Evolution (DE), as well as numerous novel intelligent optimization strategies aimed at enhancing performance and efficiency [4].

To further refine the effectiveness of SI algorithms in ELD, various enhancements have been proposed in the literature. Hassan et al. introduced the Enhanced Social Network Search (ESN) algorithm, which optimizes search strategies through a "high-low speed ratio" mechanism to strengthen global search capabilities while mitigating premature convergence [5]. Abhishek et al. developed Cognitive Team Optimization (CTO), which integrates a remedial hierarchy framework to enhance the search capability of low-fitness individuals, leading to superior performance in both ELD and Combined Economic and Emission Dispatch (CEED) problems [6]. Hao et al. proposed an Arithmetic Optimization Algorithm (AOA) that incorporates elementary function perturbation, thereby reinforcing global search efficiency and expediting convergence [7].

In addition, Al-Betar et al. introduced a hybrid optimization framework by integrating the Grey Wolf

Manuscript received March 31, 2025; revised May 30, 2025. This work was supported by the Basic Scientific Research Project of Institution of Higher Learning of Liaoning Province (Grant No. LJ222410146054), and Postgraduate Education Reform Project of Liaoning Province (Grant No. LNYJG2022137).

Hao-Ming Song is a doctoral student of School of Electronic and Information Engineering, University of Science and Technology Liaoning, Anshan, 114051, P. R. China (e-mail: shm@stu.ustl.edu.cn).

Jie-Sheng Wang is a professor of School of Electronic and Information Engineering, University of Science and Technology Liaoning, Anshan, 114051, P. R. China (Corresponding author, phone: 86-0412-2538246; fax: 86-0412-2538244; e-mail: wjs@ustl.edu.cn).

Xin-Yi Guan is a postgraduate student at School of Electronic and Information Engineering, University of Science and Technology Liaoning, Anshan, 114051, P. R. China (e-mail: gxy@stu.ustl.edu.cn).

Jia-Hui Zhao is a postgraduate student at School of Electronic and Information Engineering, University of Science and Technology Liaoning, Anshan, 114051, P. R. China (e-mail: zjh@stu.ustl.edu.cn).

Optimizer (GWO) with Beta Hill Climbing (βHC), achieving a dynamic equilibrium between exploration and exploitation to enhance solution quality [8]. Tribhuvan et al. proposed a Chaos-Based Slime Mould Algorithm (CSMA), which leverages chaotic maps to improve stability and competitiveness in handling ELD problems [9]. Zhang et al. enhanced the Pelican Optimization Algorithm (POA) by incorporating a vertical crossover operator, an elite-guided perturbation strategy, and a variable dimension mechanism, significantly improving population diversity and the algorithm's ability to escape local optima [10].

Moreover, Pan et al. developed the Multi-Group Marine Predators Algorithm (MGMPA), which employs a multi-population framework with periodic information exchange, demonstrating remarkable cost reductions in ELD applications [11]. Yang et al. proposed an Improved Whale Optimization Algorithm (IWOA) by introducing an adaptive nonlinear inertia weight mechanism and limited mutation strategies, leading to enhanced convergence speed and global search efficiency [12]. Furthermore, Hassan et al. introduced the Leader White Shark Optimizer (LWSO), which incorporates a leadership-based exploitation mechanism, significantly improving convergence performance and search efficiency [13].

These advancements highlight the continuous evolution of SI-based optimization techniques, reflecting their increasing effectiveness in addressing complex, large-scale ELD problems with nonlinear constraints and multiple objectives. By integrating adaptive mechanisms, hybrid strategies, and multi-population frameworks, researchers have progressively enhanced the balance between exploration and exploitation, ultimately improving the robustness and accuracy of power dispatch solutions.

The Chinese Pangolin Optimizer (CPO) [14], inspired by pangolin predation, exhibits strong stability and convergence in complex optimization tasks. However, its application to constrained problems like ELD remains limited by susceptibility to local optima and restricted search accuracy. To address these issues, this study proposes an improved CPO integrating a probability-oscillating convergence factor strategy to enhance its performance in ELD. The proposed approach is validated through multiple test cases, demonstrating its effectiveness.

II. Economic Load Dispatch

A. Objective Function

The main goal of the Economic Load Dispatch (ELD) problem is to optimally allocate power generation among various units to minimize costs, while satisfying the total electricity demand during the specified time period. This optimization is subject to constraints, including power balance and generator operational limits. Typically, the fuel cost for each generation unit is modeled using a smooth quadratic polynomial function, as shown in Eq. (1).

$$MinF_i = \sum_{i=1}^{n} (\alpha_i + \beta_i P + \gamma_i P_i^2) \quad (1)$$

where, *Fi* represents the total fuel cost, while *Pi* indicates the power output of the *i*-th generator, with *n* denoting the total number of generating units. The constants α_i, β_i and γ_i are the fuel cost coefficients specific to the *i*-th generator. In steam turbines, the steam flow through control valves creates a ripple effect, making it crucial to incorporate the valve-point effect into the fuel cost model [15]. Therefore, the actual fuel cost as a function of power output is generally expressed as a combination of a quadratic polynomial and a sinusoidal component, as described by the following equation:

$$MinF_i = \sum_{i=1}^{n} (\alpha_i + \beta_i P + \gamma_i P_i^2 + |e_i \times sin(f_i(P_i^{min} - P_i))|) \quad (2)$$

where, e_i and f_i represent the coefficients associated with the valve-point effect for the *i*-th generator, while P_i^{min} denotes the minimum permissible power output of the *i*-th generating unit.

B. Constraint Handling

1) Power Balance Constraint

The power balance constraint can be mathematically represented as:

$$\sum_{i=1}^{n} P_i = P_D + P_L \quad (3)$$

where, *n* denotes the total number of generating units, P_D represents the total actual power demand, and P_L corresponds to the overall transmission loss within the system. The traditional loss calculation formula is presented as follows:

$$P_L = \sum_{i=1}^{n} \sum_{j=1}^{n} P_i B_{ij} P_j + \sum_{i=1}^{n} B_{0i} P_i + B_{00} \quad (4)$$

where, *n* denotes the total number of generating units, B_{ij} represents the loss coefficient associated with the *ij*-th element in the symmetric matrix, B_{0i} is the loss coefficient vector corresponding to the *i*-th generating unit, and B_{00} is the constant loss coefficient.

2) Generator Power Constraints

Each thermal generating unit operates within a predefined power output range, constrained by minimum and maximum generation limits. The generated power must not exceed the specified upper limit and must remain above or equal to the designated lower threshold for the respective unit. This constraint can be mathematically formulated as follows:

$$P_i^{min} \le P_i \le P_i^{max} \quad (5)$$

where, P_i denotes the power output of the *i*-th generating unit, while P_i^{min} and P_i^{max} correspond to the lower and upper operational limits of the *i*-th generator, respectively.

3) Prohibited Operating Zone

A generating unit may exhibit restricted operating regions within its input-output characteristic curve due to inherent physical limitations, such as mechanical vibrations in variable-speed bearings or malfunctions in the generator and its associated components. Consequently, each generator must be prevented from functioning within these prohibited zones. In real-world applications, the permissible operational range of the *i*-th generator can be mathematically expressed as follows:

$$P_i = \begin{cases} P_i^{min} \le P_i \le P_{i.1}^{l} \\ P_{i.k-1}^{u} \le P_i \le P_{i.k}^{l}, k = 2,3,\dots,n_i, i = 1,2,\dots,n \\ P_{i.n_i}^{u} \le P_i \le P_i^{max} \end{cases} \quad (6)$$

where, n denotes the total number of generating units, while k represents the number of restricted operating zones for the i-th generator. The parameters $P_{i,k}^{l}$ and $P_{i,k}^{u}$ correspond to the lower and upper boundaries of the k-th prohibited operating region, respectively.

III. Chinese Pangolin Optimizer Based on Probability Oscillation Convergence Factor

A. Chinese Pangolin Optimizer

1) Mathematical Model of Aroma

In the natural environment, the Chinese pangolin primarily relies on its highly developed sense of smell to locate ants or emits its own scent to lure them. A higher detected concentration of ant-related odors signifies proximity to the prey, enhancing the likelihood of a successful hunt. Conversely, a stronger pangolin-emitted scent perceived by ants increases the probability of attracting them, thereby improving capture efficiency. To effectively replicate this predatory mechanism, it is crucial to develop a mathematical model based on aroma diffusion and fusion. The corresponding mathematical representation is given as follows:

$$M(x,y,z) = R(x)e^{-ay^2}e^{-bz^2} \tag{7}$$

where, $\mathrm{R(x)} = \frac{\mathrm{Q}}{2\pi u\sigma_y\sigma_z}$ denotes the pollutant concentration distribution along the x-axis, influenced by factors such as emission source intensity, wind velocity, and diffusion coefficient, thereby modeling the dispersion and dilution behavior of pollutants during propagation.

In the vertical dimension, the parameters σ_y and σ_z represent the fusion coefficients along the y-axis and z-axis, respectively, and can be determined using the following expressions:

$$\begin{cases} \sigma_y^2 = \frac{\int_0^\infty y^2 M(x,y,z)dy}{\int_0^\infty M(x,y,z)dy} \\ \sigma_z^2 = \frac{\int_0^\infty z^2 M(x,y,z)dz}{\int_0^\infty M(x,y,z)dz} \end{cases} \tag{8}$$

The source intensity formula at the origin O is given by:

$$Q = \int_{-\infty}^{\infty}\int_{-\infty}^{\infty} uM(x,y,z)dydz \tag{9}$$

where, u represents the average wind speed. By combining Eq. (7)-(9), we can calculate the aroma concentration at any downwind point $M(x,y,z)$ as:

$$M(x,y,z) = \frac{Q}{2\pi u\sigma_y\sigma_z} exp\left[-\left(\frac{y^2}{2\sigma_y^2} + \frac{z^2}{2\sigma_z^2}\right)\right] \tag{10}$$

In practical scenarios, the Earth's surface imposes a constraint on the dispersion of aroma concentration, limiting its diffusion range. To more accurately replicate this phenomenon, the surface is assumed to function as a reflective boundary, causing aroma re-circulation. This is modeled using the image source method. According to this principle, the aroma concentration at any given point $M(x,y,z)$ is considered the cumulative effect of two contributions. In the absence of a ground boundary, both the actual source at point A and its mirrored counterpart at point B influence the concentration at point M. The point A can be expressed as follows:

$$A(x,y,z) = \frac{Q}{2\pi u\sigma_y\sigma_z} exp\left(-\frac{y^2}{2\sigma_y^2}\right) exp\left(-\frac{(z-H)^2}{2\sigma_z^2}\right) \tag{11}$$

Likewise, the aroma concentration resulting from the contribution of the image source located at point B is given by:

$$B(x,y,z) = \frac{Q}{2\pi u\sigma_y\sigma_z} exp\left(-\frac{y^2}{2\sigma_y^2}\right) exp\left(-\frac{(z+H)^2}{2\sigma_z^2}\right) \tag{12}$$

Hence, by integrating Eq. (11)-(12), the resulting aroma concentration at point M can be expressed as:

$$M(x,y,z) = A(x,y,z) + B(x,y,z) \tag{13}$$

In conclusion, the aroma concentration at point M can be represented as:

$$M(x,y,z) = \frac{Q}{2\pi u\sigma_y\sigma_z} exp\left(-\frac{y^2}{2\sigma_y^2}\right)\left[exp\left(-\frac{(z-H)^2}{2\sigma_z^2}\right) + exp\left(-\frac{(z+H)^2}{2\sigma_z^2}\right)\right] \tag{14}$$

The aforementioned equation describes a Gaussian dispersion model for aroma propagation in a constrained environment. It quantifies the aroma concentration at a specific location situated x meters downwind, y meters laterally, and z meters above the surface. In this model, Q represents the emission intensity of the aroma source, while u denotes the mean wind velocity. The parameters σ_y and σ_z correspond to the horizontal and vertical dispersion coefficients, respectively, and H represents the effective release height of the aroma source. The variables y and z define the lateral and vertical distances from the dispersion center.

The expression for calculating the aroma concentration at ground level is formulated as follows:

$$M(x,0,0) = \frac{Q}{\pi u\sigma_y\sigma_z} exp\left(-\frac{H^2}{2\sigma_z^2}\right) \tag{14}$$

$$u = 2 + r_1 \tag{15}$$

$$H = \frac{r_2}{2} \tag{16}$$

where, Q=100 denotes a constant aroma source emission rate. To precisely model aroma dispersion in accordance with the behavioral characteristics of the Chinese pangolin and ants, the effective height of the aroma source is restricted to the range of 0-0.5 m, while the mean wind speed is maintained between 2-3 m/s. Additionally, r_1 and r_2 represent random variables following a uniform distribution within the interval [0,1].

According to the P-G curve principle, as the distance decreases, the diffusion capability in the horizontal direction decreases linearly, whereas in the vertical direction, it decreases non-linearly. In other words, as the Chinese pangolin approaches the ants, σ_y exhibits a linear decline, while σ_z follows a nonlinear decrease. Therefore, in this study, σ_y and σ_z are defined as follows:

$$\sigma_y = 50 - \frac{10*t}{T} \tag{17}$$

$$\sigma_z = sin\left(\frac{\pi*t}{T}\right) + 40 * exp\left(-\frac{t}{T}\right) - 10 * ln\left(\frac{\pi*t}{T}\right) \tag{18}$$

where, t represents the current iteration, and T denotes the maximum number of iterations. To maintain the aroma concentration within the bounds of 0 and 1, Eq. (14) is subjected to a normalization procedure, which can be formulated as follows:

$$C_M(t) = \frac{M(t)-min(M)}{max(M)-min(M)} \quad (19)$$

where, $M(t)$ represents the aroma concentration at the *t*-th iteration, while $C_M(t)$ denotes the normalized aroma concentration at the same iteration.

2) Initialization

The population is thus defined as:

$$X = \begin{bmatrix} x_{1,1} & x_{1,2} & \cdots & x_{1,d} \\ x_{2,1} & x_{2,2} & \cdots & x_{2,d} \\ \vdots & \vdots & \vdots & \vdots \\ x_{n,1} & x_{n,2} & \cdots & x_{n,d} \end{bmatrix} \quad (20)$$

where, n represents the population size, and d denotes the number of dimensions of the variables. X signifies the current population of candidate solutions, where each solution is randomly initialized within the specified upper bound (UB) and lower bound (LB) of the problem, as expressed by:

$$X_{ij} = rand \times (UB_j - LB_j) + LB_j, i = 1,2,\ldots,n, j = 1,2,\ldots,\mathrm{d} \quad (21)$$

where, UB_j represents the upper bound of the *j*-th component of the given problem, while LB_j denotes the lower bound of the *j*-th component, expressed as:

$$\begin{cases} UB = [ub_1, ub_2, \ldots, ub_d,] \\ LB = [lb_1, lb_2, \ldots, lb_d,] \end{cases} \quad (22)$$

In CPO, during the hunting process, the Chinese pangolin primarily utilizes its acute sense of smell to assess the aroma concentration emitted by nearby ants. Guided by its predatory instincts, it subsequently determines whether to engage in luring or predation behavior. In the natural environment, the Chinese pangolin typically exhibits both behaviors concurrently over a period of time to enhance its prey capture efficiency. This process can be mathematically represented as:

$$\begin{cases} C_M \geq 0.2,\ r_1 \leq 0.5,\ Lurning\ behavior \\ C_M < 0.7 || r_1 > 0.5,\ Predation\ behavior \end{cases} \quad (23)$$

where, C_M represents the aroma concentration. When $0.2 \leq C_M < 0.7$, it indicates that the Chinese pangolin engages in both behaviors simultaneously. r_1 is a random number within the range [0,1].

3) Mathematical Model of Luring Behavior

The attraction behavior of CPO is divided into two phases: the attraction and capture phase, and the movement and feeding phase ($C_M(t) \geq 0.2 \& \& r_1 \leq 0.5$).

Case 1: Attraction and Capture Stage.

During this phase, the Chinese pangolin emits its scent to attract ants, which follow the scent trail and move closer until they are captured by the pangolin. In this scenario, the positional dynamics between the pangolin and the ants are primarily determined by factors such as the ants' movement behavior, the scent path, fatigue levels, and energy variations. The mathematical model representing this stage can be expressed as:

$$D_A(t) = |a \cdot X_A(t) - X_M(t)| \quad (24)$$

$$X_A(t+1) = X(t) + X_A(t) - A_1 \cdot D_A(t) \quad (25)$$

In Eq. (24), the relative positional change between the ant and the Chinese pangolin, influenced by the emitted scent trajectory, is simulated. Eq. (25) models the energy expenditure of the ant as it follows the scent path. Specifically, as the ant progressively approaches the Chinese pangolin, $X_A(t)$ represents the ant's position at the *t*-th iteration, and $X_M(t)$ indicates the position of the Chinese pangolin at the same iteration. $D_A(t)$ denotes the relative distance between the ant and the pangolin at the *t*-th iteration. In Eq. (24), a is the scent trajectory factor, simulating the ant's gradual approach toward the pangolin under the influence of the emitted scent trail. The motion equation governing this behavior in three-dimensional space can be simplified as:

$$\begin{cases} a_x = x(t) + r_2 \times \sqrt{2D_c \frac{1}{T}} \\ a_y = y(t) + r_2 \times \sqrt{2D_c \frac{1}{T}} \\ a_z = z(t) + r_2 \times \sqrt{2D_c \frac{1}{T}} \end{cases} \quad (26)$$

$$a = \sqrt{a_x^2 + a_y^2 + a_z^2} \quad (27)$$

where, a_x, a_y, and a_z represent the perturbations in the scent position along the x, y and z axes after each iteration, respectively. Meanwhile, $x(t)$, $y(t)$, and $z(t)$ denote the scent position along the x, y, and z directions at the *t*-th iteration. $r_2 \in randn()$ represents a random number drawn from a standard normal distribution. D_c denotes the diffusivity of the scent, which is empirically set to 0.6 in this study. T represents the maximum number of iterations. Eq. (21) integrates the Brownian motion model with the tracking factor, effectively capturing the complex dynamics of how ants perceive and pursue the scent. This integration results in a three-dimensional scent trajectory.

In Eq. (20), A_1 represents the energy fluctuation factor, which simulates the energy variations of ants due to fatigue as they approach the Chinese pangolin. Its equation can be simplified as:

$$A_1 = 2 \times E \times rand() - E \quad (28)$$

where, E represents the energy consumption factor, which is defined as:

$$E = exp(-\lambda \times V_{O2} \times t \times (1 + Fatigue)) \quad (29)$$

where, $\lambda = 0.1 \times rand()$ is the energy adjustment factor, $V_{O2} = 0.2 \times rand()$ denotes oxygen consumption, and $Fatiue$ represents the fatigue index, expressed as:

$$Fatigue = log(\frac{t \times \pi + T}{T}) \quad (30)$$

where, t denotes the current iteration, while T represents the total number of iterations.

Case 2: Movement and Feeding Phase. During this phase, the Chinese pangolin captures the ants and swiftly moves toward the nearest water source, such as a stream or pond. Upon reaching the water's edge, the pangolin enters the water, sheds its scales, and uses its elongated tongue to consume the ants that are on the water's surface. The mathematical representation associated with this phase can be expressed as follows:

$$D_M(t) = |C_1 \cdot D_A(t) - X_M(t)| + L_{levy} \cdot (1 - \frac{t}{T}) \quad (31)$$

$$X_M(t+1) = X(t) + X_M(t) - A_1 \cdot D_M(t) \quad (32)$$

$D_M(t)$ is the relative distance between the Chinese pangolin and the river (the optimal position) at the *t*-th iteration. $D_A(t)$ denotes the relative distance between the ants and the Chinese pangolin at the *t*-th iteration. $X_M(t)$ represents the position of the Chinese pangolin at the *t*-th iteration. A_1 is the energy fluctuation factor, calculated using Eq. (28). C_1 represents the fast reduction factor, which describes the Chinese pangolin's rapid approach to the river as the iterations progress and can be computed using Eq. (33).

$$C_1 = 2 - t \times (\frac{2}{T}) \quad (33)$$

L_{levy} represents the step size of the Levy flight function, employed to model the random movement path of the Chinese pangolin as it approaches the river. The corresponding equation can be expressed as:

$$L_{levy} = s \times \frac{u \times \sigma}{|v|^{\frac{1}{\beta}}} \quad (34)$$

where, β is a random variable within the interval [0, 2] (referred to as $\beta = 1.5$ in this study). *s* is a constant with a fixed value of 0.01. *u* and *v* are random variables within the range [0, 1], and σ is defined as:

$$\sigma = (\frac{\Gamma(1+\beta) \times sin(\frac{\pi\beta}{2})}{\Gamma(\frac{1+\beta}{2}) \times \beta \times 2^{\frac{\beta-1}{2}}}) \quad (35)$$

Ultimately, during the luring phase, the position of the Chinese pangolin is updated according to Eq. (31).

$$X(t+1) = \frac{X_M(t) + X_A(t)}{2} + \frac{r_2^3 \cdot sin(X_A(t) \cdot e^{t/T})}{4\pi \cdot tan(X_M(t) \cdot e^{\frac{4\pi^2 t}{T}})} \quad (36)$$

where, *r* is a random number in the range [0,1].

4) Mathematical Model of Predation Behavior

Case 1: Search and Localization Phase ($0 \leq CM < 0.3$). The corresponding mathematical model for this phase is given by:

$$D_M(t) = \left|L_{levy} \cdot X_M(t) - X(t)\right| \quad (37)$$

$$D_M(t+1) = sin(C_1 \cdot X(t) + A_1 \cdot \left|X_M(t) - L_{levy} \cdot D_M(t)\right|) \quad (38)$$

where, $D_M(t)$ denotes the relative distance between the pangolin and the nest (the optimal position) at the *t*-th iteration.

Case 2: Rapid Approach Stage ($0.2 \leq CM < 0.6$). The corresponding mathematical model for this stage is expressed as:

$$D_M(t) = |a \cdot X_M(t) - X(t)| \quad (39)$$

$$X_M(t+1) = X(t) - A_1 \cdot |X_M(t) - exp(-a) \cdot sin(rand \cdot \pi) \cdot D_M(t)|) \quad (40)$$

Eq. (39) illustrates the difference in distance between the fragrance trajectory of the Chinese pangolin and the location of the ant nest at the *t*-th iteration. In Eq. (40), *a* denotes the fragrance trajectory factor, which is derived from Eq. (26), and L_{levy} represents the step size of the Lévy flight function, which can be computed using Eq. (34).

Case 3: Digging and Feeding Stage ($CM \geq 0.6$). The mathematical model for this stage is:

$$D_M(t) = |C_1 \cdot X_M(t) - X(t)| \quad (41)$$

$$X(t+1) = X(t) + A_1 \cdot |X_M(t) - D_M(t)| \quad (42)$$

Ultimately, during the predation phase, the position of the Chinese pangolin is modified according to Eq. (43).

$$X(t+1) = C_1 \cdot X_M(t) \quad (43)$$

In conclusion, the Chinese pangolin utilizes its keen sense of smell and unique hunting behaviors, including both attraction and predation, to capture ants.

B. Chinese Pangolin Algorithm Based on the Probability Oscillation Convergence Factor Strategy

Due to the tendency of the original CPO algorithm to get trapped in local optima during the iteration process and its limited search accuracy, we propose the Probability Oscillation Convergence Factor Strategy. This strategy adjusts the search range and search form in Eq. (28). In the Probability Oscillation Convergence Factor Strategy, we incorporate several probability distributions, including uniform, beta, exponential, normal, Rayleigh and Weibull distributions, to enhance the initial exploration capability of the Chinese Pangolin Optimizer (CPO). This approach aims to improve the algorithm's ability to avoid local optima, expedite the convergence process, and increase the overall optimization accuracy. The introduction of mathematical distribution is able to dynamically adjust the fitness value so that it is in the sampling density of promising regions, enabling targeted refinement and focusing on high-quality regions.

For statistical convenience, we label the proposed different distributions as CPO1-CPO6. The original CPO image is shown in Fig. 1, and the formulas for the Probability Oscillation Convergence Factor Strategy are given in Eq. (44)-(45). The image with the introduction of the Probability Oscillation Convergence Factor Strategy is shown in Fig. 2.

$$C_1 = (2 - t \times (\frac{2}{T})) * s \quad (44)$$

$$s = (1 + W \cdot (1 - \frac{t}{T})) \quad (45)$$

In the equation, *s* represents the introduced Probability Oscillation Convergence Factor, and the specific information for *W* is provided in TableI.

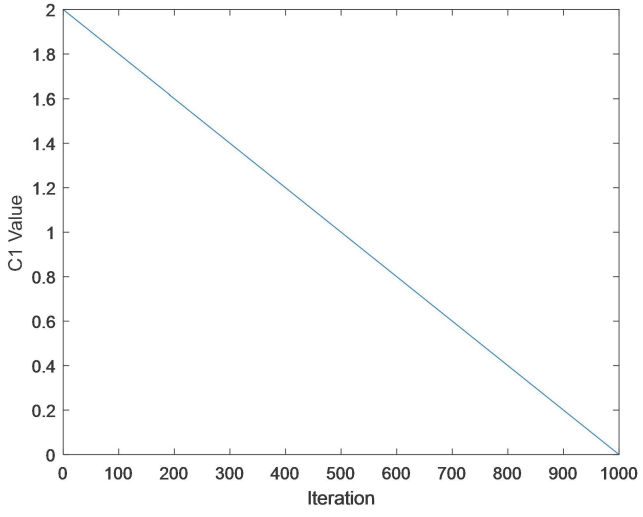

Fig. 1 C_1 image.

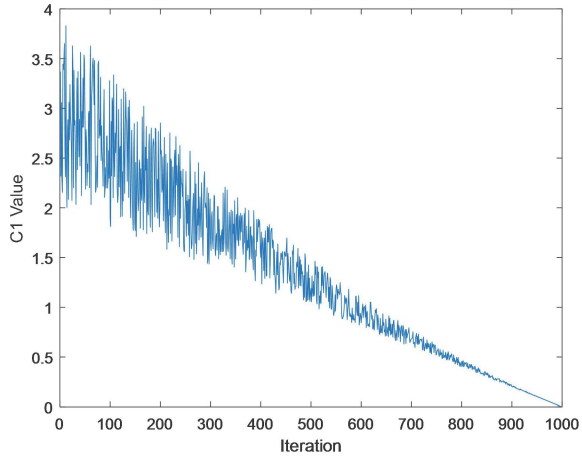

(1) ICPO1

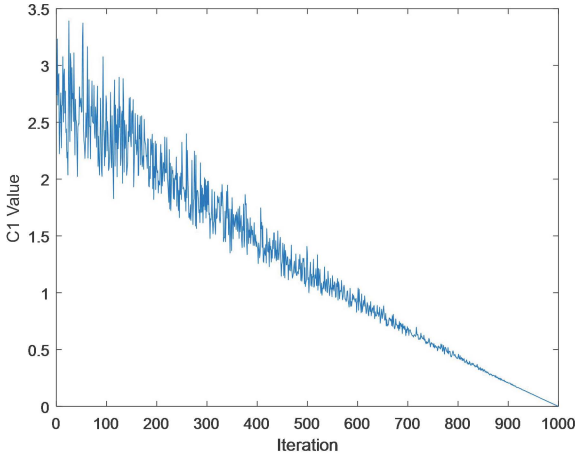

(2) ICPO2

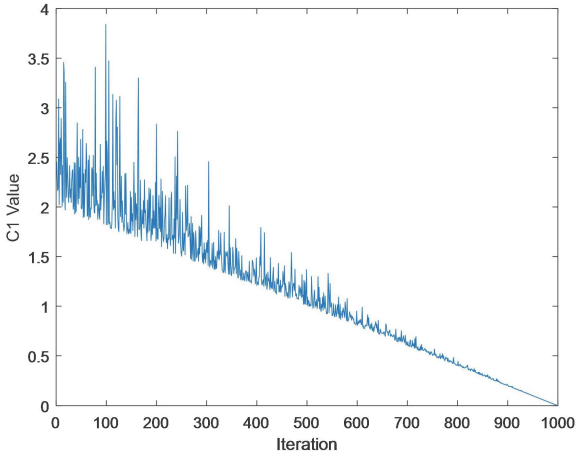

(3) ICPO3

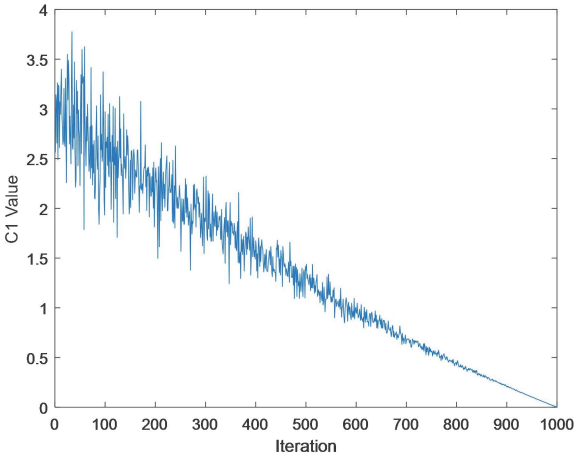

(4) ICPO4

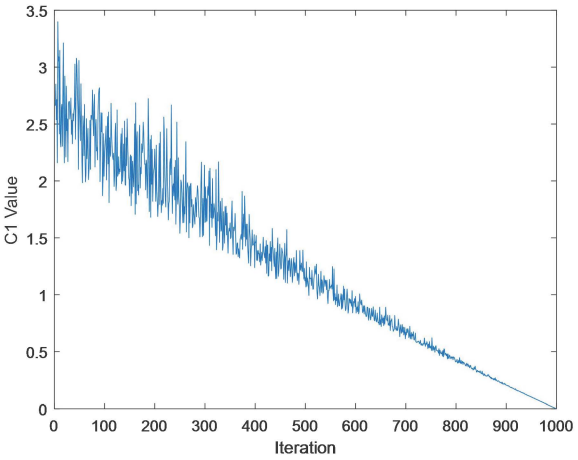

(5) ICPO5

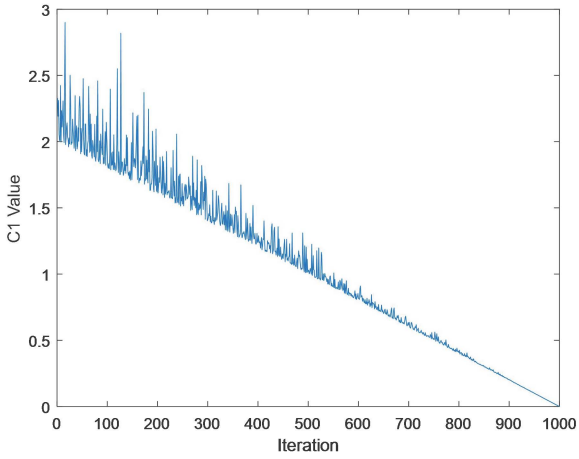

(6) ICPO6

Fig. 2 Improved C_1 image.

TABLE I. PROBABILITY OSCILLATION CONVERGENCE FACTORS

Name	Distribution type	W	Parameter setting
ICPO1	Uniform distribution	Rand	--
ICPO2	Beta distribution	Betarnd (a,b)	a=3, b=5
ICPO3	Exponential distribution	Exprnd (a)	a=0.2
ICPO4	Normal distribution	Normrnd (a,b)	a=0.5, b=0.1938
ICPO5	Rayleigh distribution	Raylrnd (a)	a=0.27
ICPO6	Weibull distribution	Wblrnd (a,b)	a=0.1, b=0.9

C. Flowchart and Pseudo-code of CPO Algorithm Based on Probability Oscillation Convergence Factor Strategy

The pseudo-code of the CPO algorithm is as follows:

Inputs: The population size n, maximum number of iterations T and variable dimension d

Outputs: The location of Chinese pangolin X_{best} and its fitness value

01: Initialize the random population $X_i(i = 1,2,\ldots,n)$
02: **While** (t<T) **Do**
03: Calculate the fitness values of Chinese pangolin
04: Update the aroma concentration C_M using Eq. (14)-(19)
05: Update the rapid decrease factor C_1 using Eq. (33)
06: Update the aroma trajectory factor a using Eq. (26)-(27)
07: Update the Levy's flight function step length L_{levy} using Eq. (34)-(35)
08: X_M = best position (Chinese pangolin position)
09: X_A = second best position (Ant position)
10: **For** (each Chinese pangolin position (X_i)) **Do**
11: Update the energy fluctuation factor A_1 using Eq. (28)

12: Update the energy consumption factor E using Eq. (29)
13: Update the fatigue index factor $Fatigue$ using Eq. (30)
14: Update the random r_1
/*Luring Behavior*/
15: **If** $(C_M \geq 0.2 \&\& r_1 \leq 0.5)$ **Then**
16: Update the location vector using Eq. (24)-(25)
// Attraction and Capture Stage
17: Update the location vector using Eq. (31)-(32)
// Movement and Feeding Stage
18: Update Eq. (36) update the best position X^*
/*Predation Behavior*/
19: **Else If** $(C_M \leq 0.7 \parallel r_1 \leq 0.5)$ **Then**
20: **If** $(0 \leq C_M < 0.3)$ **Then**
21: Update the location vector using Eq. (37)-(38)
// Search and Localization Stage
22: Using Eq. (42) update the best position X^*
23: **Else If** $(0.3 \leq C_M < 0.6)$ **Then**
24: Update the location vector using Eq. (39)-(40)
// Rapid Approach Stage
25: Using Eq. (43) update the best position X^*
26: **Else If** $(C_M \geq 0.6)$ **Then**
27: Update the location vector using Eq. (41)-(42)
// Digging and Feeding Stage
28: Using Eq. (43) update the best position X^*
29: **End If**
30: **End If**
31: **End For**
32: t=t+1
33: **End While**
34: Return the best position X^* and its fitness value

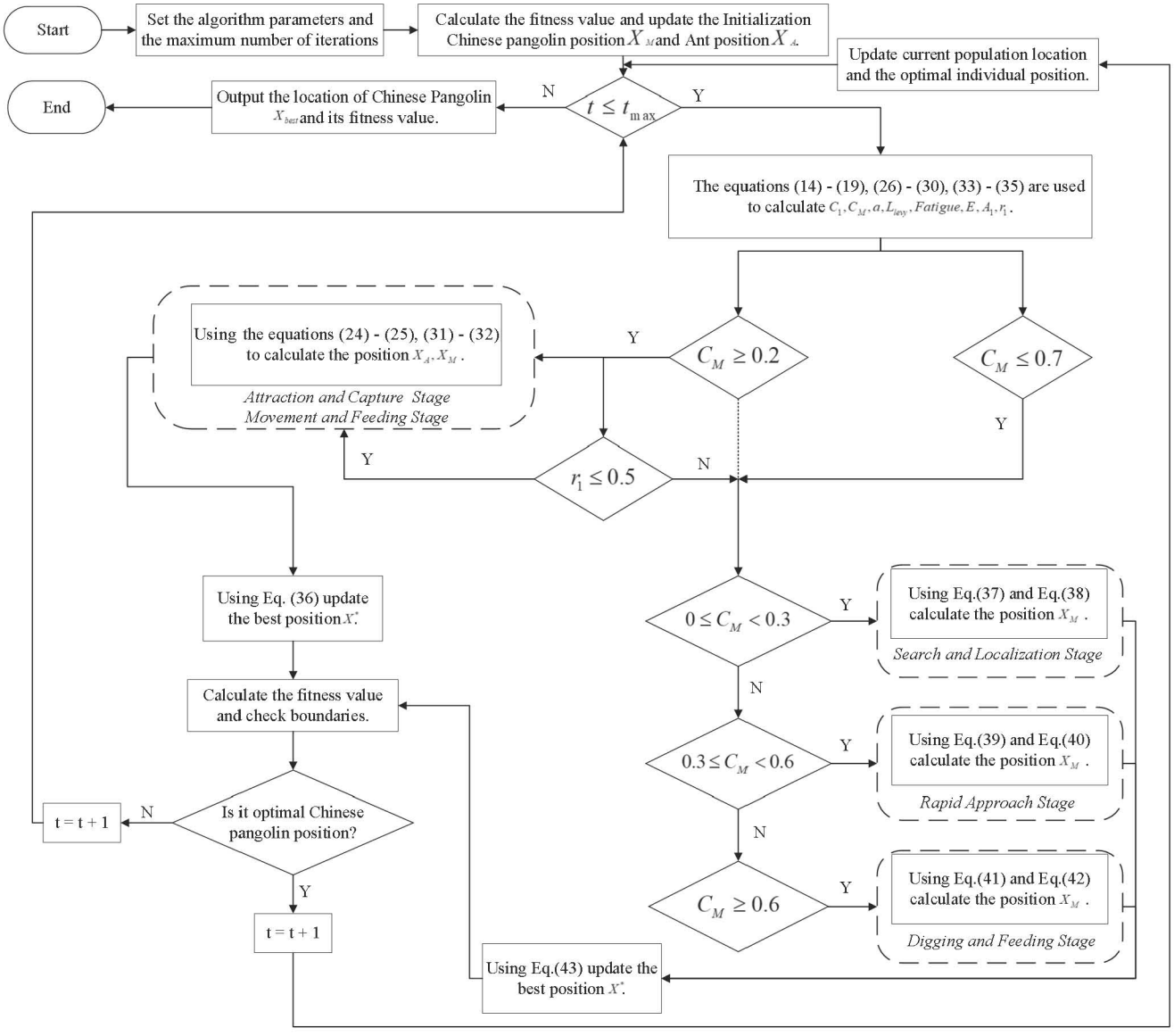

Fig. 3 CPO flow chart.

IV. Simulation Experiment and Result Analysis

This section provides a thorough performance assessment of the Improved Chinese Pangolin Optimizer (ICPO), enhanced with the Probability Oscillation Convergence Factor strategy to improve its global search capability and convergence robustness. The evaluation is based on the 12 benchmark functions from the CEC-2022 competition, which are widely used for testing optimization algorithms. These functions encompass different problem types, including unimodal (F1), basic multimodal (F2-F5), hybrid (F6-F8) and composite (F9-F12). Each test function has a dimensionality of 20, and each algorithm is allowed a maximum of 1000 iterations. To ensure the statistical validity of the results, each algorithm is independently executed 30 times, with the outcomes averaged across runs, including the best solutions,

mean fitness values, and standard deviations.

Fig. 4 illustrates the convergence behavior of various algorithms across these benchmark functions. The results indicate that the ICPO algorithm, enhanced with the Probability Oscillation Convergence Factor strategy, consistently outperforms the original CPO in most test cases. While slight under-performance is observed in a few functions, the overall results suggest that the proposed strategy significantly improves the global search capability and mitigates premature convergence, enhancing the algorithm's stability in convergence.

A closer examination of the statistical results in Table II indicates that the original CPO algorithm does not attain optimal performance in any of the benchmark test functions. It consistently under-performs compared to the enhanced versions in terms of best solutions, mean values, and standard deviations. This suggests that the original CPO has a propensity to converge prematurely to local optima, restricting its capacity to thoroughly explore and exploit the solution space. In contrast, the integration of the Probability Oscillation Convergence Factor strategy leads to considerable improvements in the performance of the modified variants (ICPO1-ICPO6), as they exhibit notable advancements across several test functions.

For instance, ICPO1 achieves the best mean values for F3, F8 and F10, the smallest standard deviations for F2 and F11, and the optimal solutions for F3, F6 and F11, indicating its strong performance in handling complex multi-modal and hybrid optimization problems. ICPO2 shows the best mean performance on F6 and achieves the optimal solutions for F7 and F9, demonstrating its powerful global search capability in high-dimensional problems. ICPO3 attains the best mean values for F2 and F11, the lowest standard deviation for F8, and the optimal solutions for F2 and F12, suggesting its efficiency in solving composite optimization problems. ICPO4 outperforms other variants in terms of mean values for F1, F4, F7 and F12, exhibits the lowest standard deviations for F1, F3 and F10, and finds the optimal solution for F11, highlighting its stable convergence characteristics. ICPO5 records the best mean value for F9, the smallest standard deviations for F5, F7 and F9, and the optimal solution for F1, reflecting its high precision in certain function landscapes. ICPO6 achieves the best mean fitness for F5, the lowest standard deviations for F4, F6 and F12, and the optimal solutions for F4, F5 and F8, showcasing its strong adaptability to hybrid and composite functions.

In order to more obviously compare the performance superiority of ICPO, the stacked graph in line is drawn according to the average fitness value ranking of each algorithm, and each algorithm corresponds to an image, as shown in Fig. 5. The smaller the area in the image, the higher the overall ranking of the corresponding algorithm. Overall, the ICPO variants exhibit distinct strengths across different test functions. ICPO1 and ICPO4 consistently achieve the best mean values in multiple test cases, indicating fast convergence and stable optimization performance. ICPO2 and ICPO3 are more effective at discovering optimal solutions, demonstrating their strong ability to explore the search space and escape local optima. Meanwhile, ICPO5 and ICPO6 frequently show the smallest standard deviations, indicating their robustness and solution stability in certain problem instances. A closer look at specific functions further demonstrates the suitability of particular ICPO variants for different problem landscapes.

In conclusion, the experimental results confirm that the ICPO series significantly enhances the optimization capabilities of the original CPO algorithm. The proposed improvements lead to substantial gains in convergence speed, global search ability, and solution stability. The varying strengths of different ICPO variants across the benchmark functions suggest that each modification strategy is particularly effective for specific types of optimization problems. Therefore, in practical applications, selecting the appropriate ICPO variant based on the specific characteristics of the optimization problem can lead to superior performance and more reliable solutions.

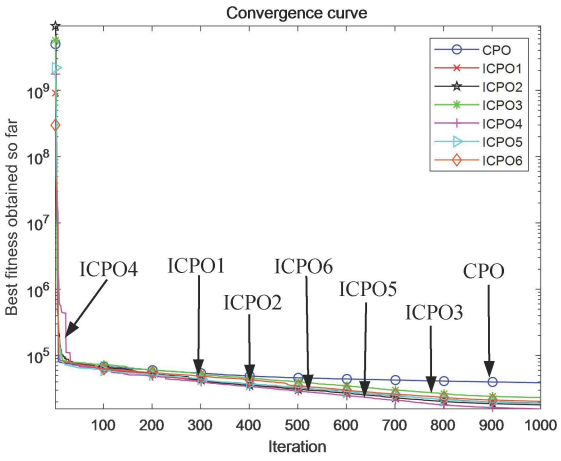

(1) f_1

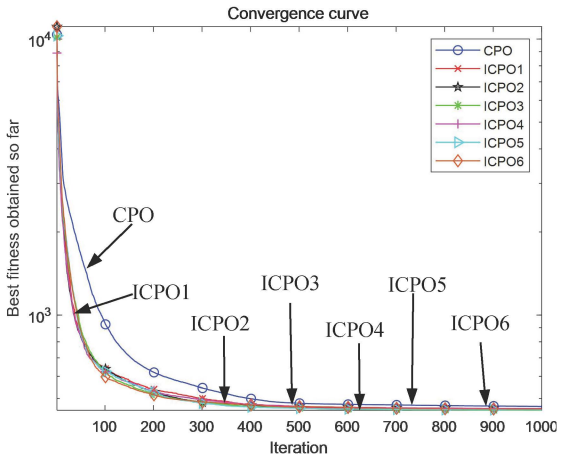

(2) f_2

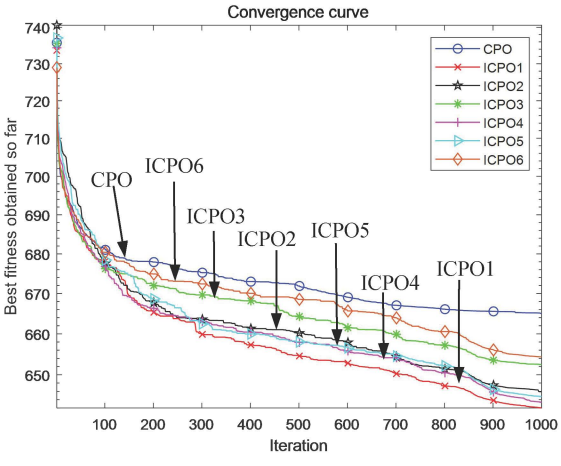

(3) f_3

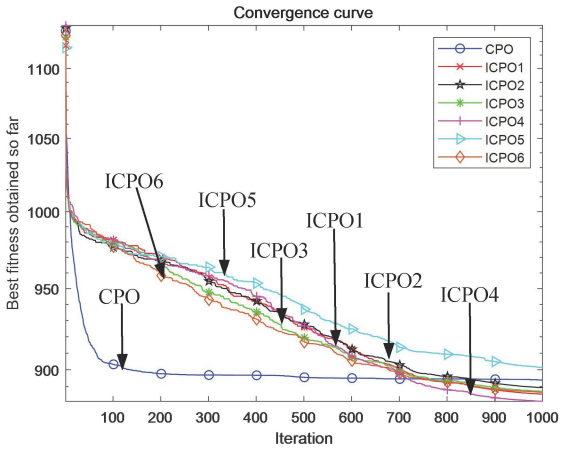

(4) f_4

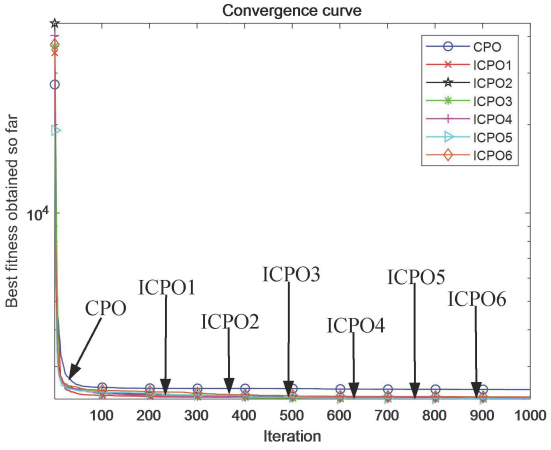

(8) f_8

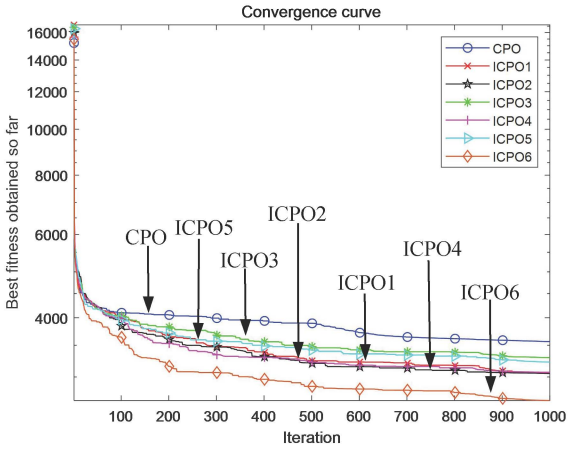

(5) f_5

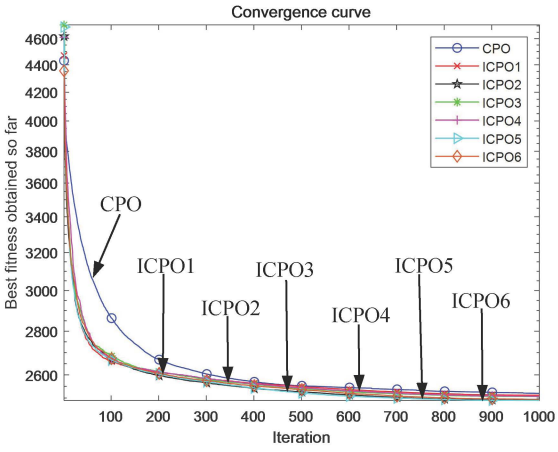

(9) f_9

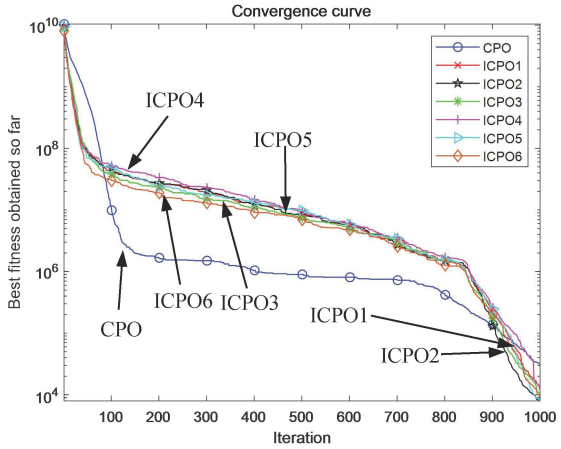

(6) f_6

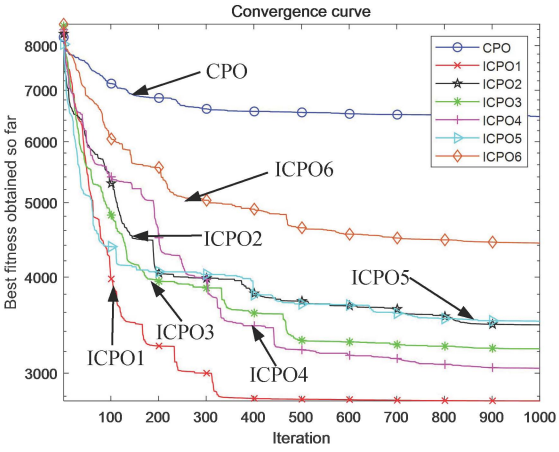

(10) f_{10}

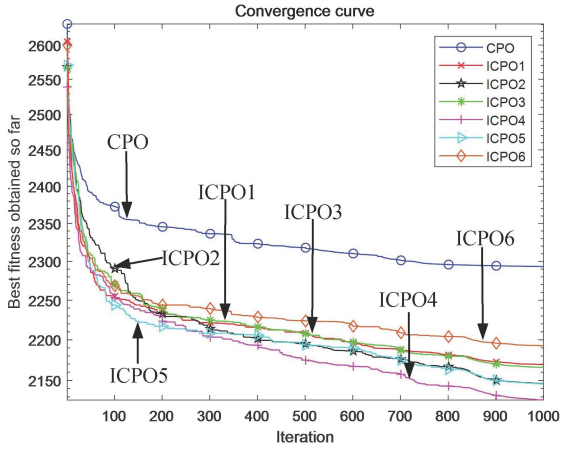

(7) f_7

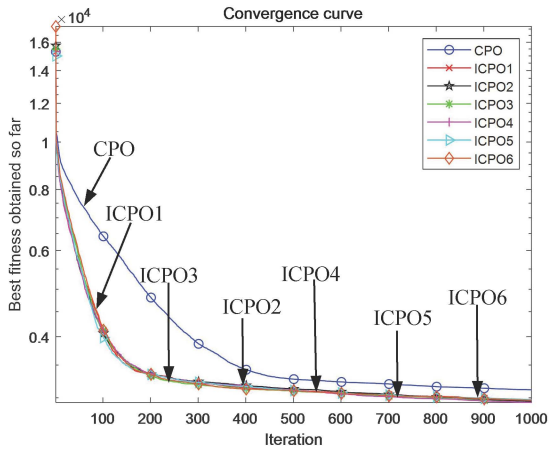

(11) f_{11}

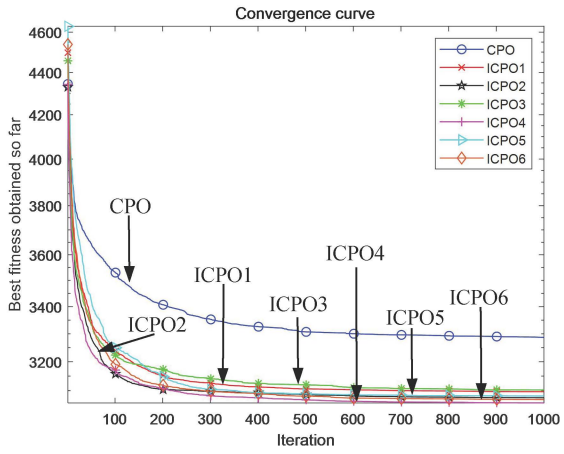

(12) f_{12}

Fig. 4 Convergence diagram of experimental results.

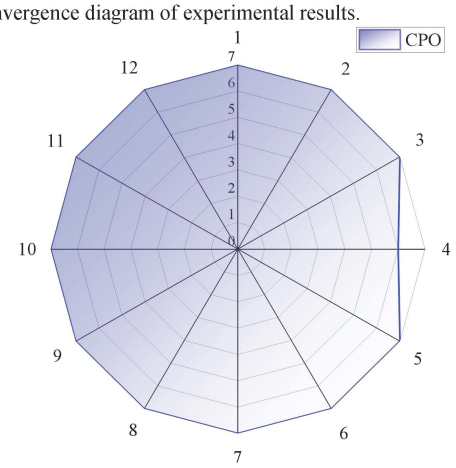

(1) CPO

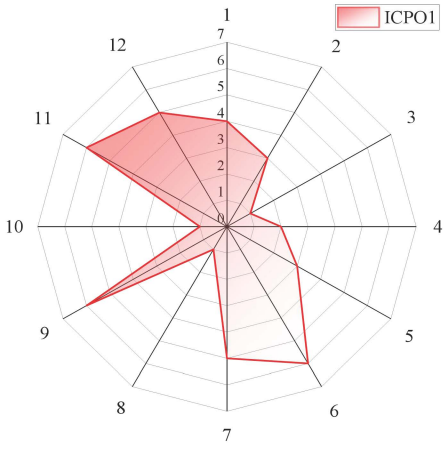

(2) ICPO1

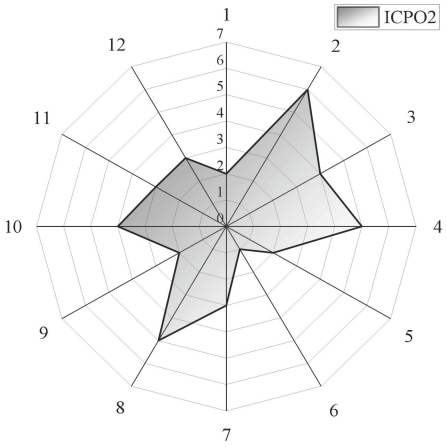

(3) ICPO2

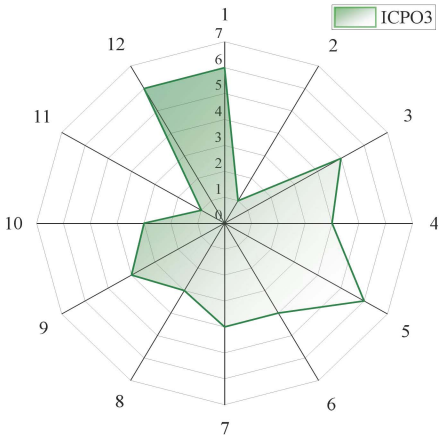

(4) ICPO3

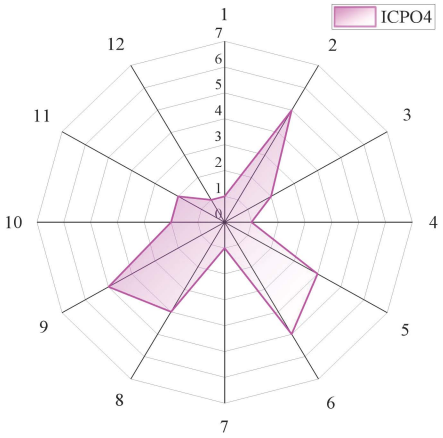

(5) ICPO4

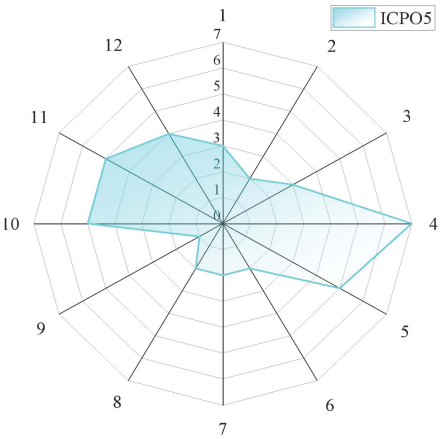

(6) ICPO5

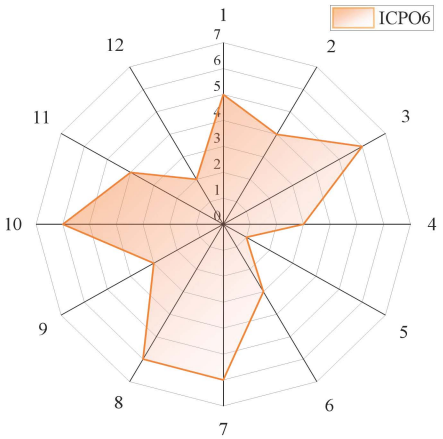

(7) ICPO6

Fig. 5 In-line stacked plots of improved CPO to solve CEC-2022 functions.

V. Improve CPO Algorithm to Solve Economic Scheduling Problem

To further validate the effectiveness of the Arithmetic Optimization Algorithm (AOA) augmented with elementary function perturbation, this section applies the algorithm to address the single-objective Economic Load Dispatch (ELD) problem in power systems. The objective of the ELD problem is to minimize the total fuel cost while satisfying the operational constraints of the power generation units. Two separate scenarios are considered for evaluation: the first scenario involves a power system with 40 generating units and a total demand of 10,500 MW, while the second scenario encompasses 110 units with a total demand of 15,000 MW.

In order to evaluate the performance of the proposed algorithm, CPO3, which has demonstrated superior results in solving the benchmark functions from CEC-BC-2022, is selected and modified accordingly. This modified version is referred to as the ICPO algorithm, where the "*I*" denotes the integration of the probability oscillation convergence factor strategy. The ICPO algorithm is then compared with several well-established optimization techniques, namely the Whale Optimization Algorithm (WOA) [16], Cuckoo Optimization Algorithm (COA) [17], Harris Hawk Optimization (HHO) [18], Pelican Optimization Algorithm (POA) [19] and the original Arithmetic Optimization Algorithm (AOA) [20], to assess its relative effectiveness in solving the ELD problem.

The choice of these comparison algorithms is motivated by their established performance in solving various optimization problems, including those related to power system load dispatch. The results of these comparisons will provide a thorough evaluation of the ICPO algorithm's capabilities and offer insights into its potential for practical applications in power systems optimization.

This comparative analysis aims to provide compelling evidence of the ICPO algorithm's ability to outperform traditional optimization methods and offer a more efficient solution to the ELD problem, ensuring that the power system operates in a cost-effective and reliable manner.

A. Case 1

In this experiment, the power system is modeled with 40 generating units, which collectively meet a total power demand of 10,500 MW. The specifications of each generator, including capacity limits and operational parameters, are detailed in Table III. To assess the performance of the proposed ICPO algorithm, the experiment is repeated 20 times, ensuring statistical reliability of the results. For each run, a maximum of 1000 iterations is allowed, with a population size set at 50. The results of the experiments are summarized in Table IV, while Fig. 6 illustrates the convergence behavior over iterations. Additionally, Fig. 7 provides a comparative bar chart that highlights the cost differences between various algorithms.

The experimental findings presented in Table IV clearly indicate that the ICPO algorithm achieves the lowest total cost, amounting to $121,336.92, while effectively satisfying the power demand constraints. This result demonstrates a significant improvement over other optimization techniques in terms of minimizing the cost of power generation. As shown in Fig. 6-7, the ICPO algorithm exhibits a robust convergence trend, consistently approaching the optimal solution with a relatively faster convergence rate compared to other intelligent algorithms.

From the analysis of these results, it is evident that the China Pangolin Algorithm (ICPO), enhanced with the probability oscillation convergence factor strategy, outperforms the competing algorithms in solving the economic load dispatch problem for Case 1. This suggests that the ICPO algorithm offers superior optimization capabilities, achieving cost-efficient solutions while maintaining the required system performance. Such findings highlight the potential of ICPO in practical power system optimization tasks, where both cost-effectiveness and operational constraints must be effectively balanced.

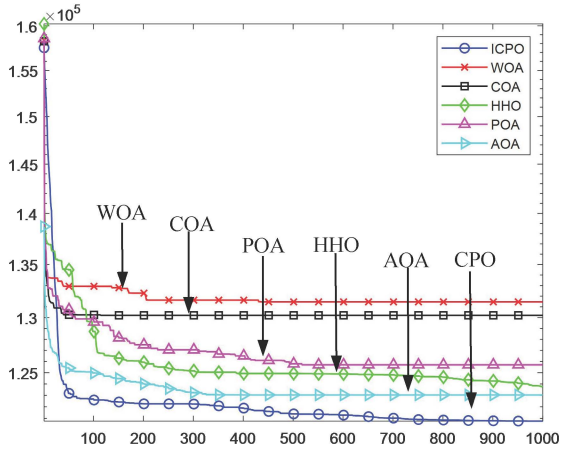

Fig. 6 Convergence diagram of experimental results for solving Case 1.

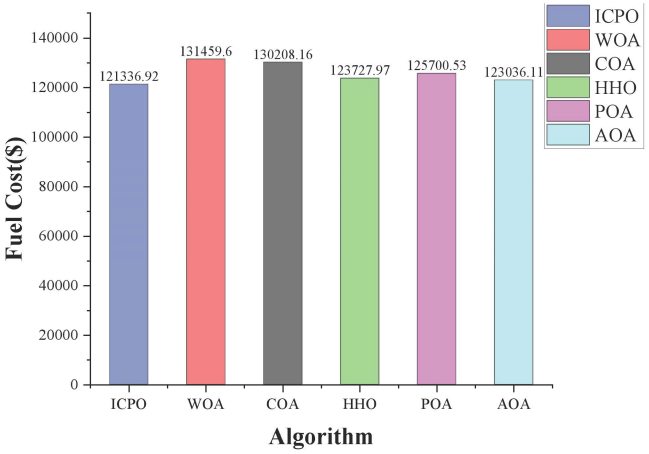

Fig. 7 Histogram of algorithm comparison in Case 1.

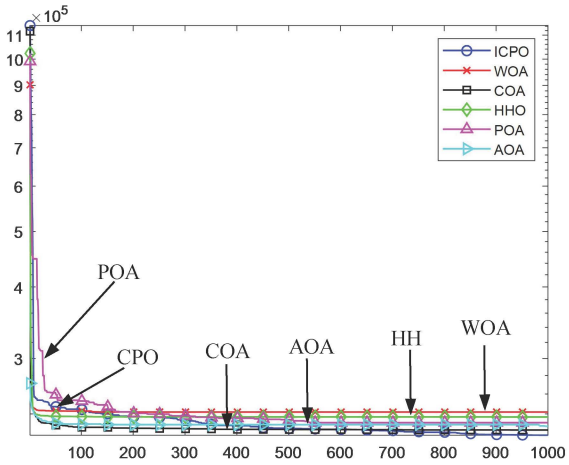

Fig. 8 Convergence diagram of experimental results for solving Case 2.

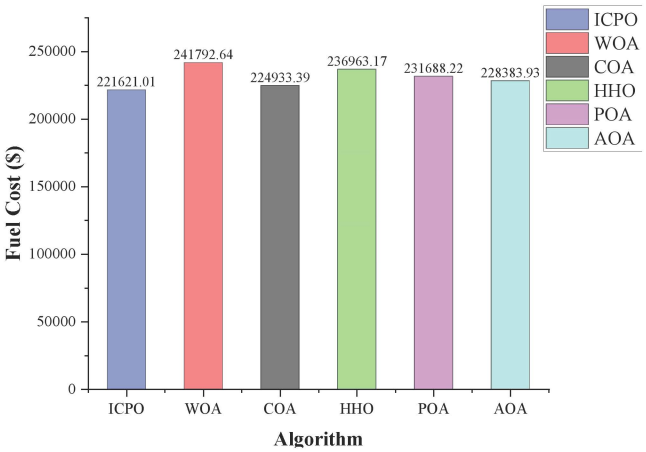

Fig. 9 Histogram of algorithm comparison in Case 2.

B. Case 2

In this scenario, the power system is composed of 110 generating units, collectively meeting a total power demand of 15,000 MW. The detailed characteristics of the generators, including their capacities, operational limits, and other relevant parameters, are provided in Table V. The experiment is executed 20 times to ensure statistical robustness, with each trial allowing for a maximum of 1000 iterations and utilizing a population size of 50. The experimental outcomes are summarized in Table VI, while Fig. 8 depicts the convergence behavior of the algorithm over the course of the iterations. Additionally, Fig. 8 presents a bar chart comparing the costs incurred by different optimization algorithms in this context.

Upon examining the data in Table VI, it is apparent that the ICPO algorithm achieves the lowest cost of $221,621.01, while simultaneously satisfying the required power demand of 15,000 MW. This outcome represents a marked improvement over the other optimization techniques in terms of minimizing the operational cost. Fig. 7-8 further illustrate the superior performance of the ICPO algorithm. The convergence graph in Fig. 8 indicates a fast and stable approach toward the optimal solution, while the bar chart in Fig. 9 highlights the ICPO algorithm's clear cost advantage relative to its competitors.

These results confirm that the China Pangolin Algorithm, enhanced with the probability oscillation convergence factor strategy, excels in solving the economic load dispatch problem for Case 2. This performance underscores the effectiveness of ICPO in optimizing large-scale power systems, where managing operational costs and adhering to power generation constraints are critical. The consistent and superior optimization demonstrated by ICPO in this case reinforces its potential as a powerful tool for real-world power system optimization tasks.

C. Time Complexity Analysis of ICPO

In the ICPO algorithm, the overall time complexity consists of two primary components: the initialization phase and the iterative optimization phase. In the initialization phase, a population of N agents with d dimensions is generated using the initialization function, which requires $O(Nd)$, and each agent's fitness is evaluated once, contributing an additional $O(Nt)$. Thus, the initialization phase has a total cost of $O(Nd + Nt)$.

In the optimization phase, the algorithm runs for T iterations. In each iteration, the positions of all agents are first boundary-checked in $O(Nd)$, and their fitness values are calculated in $O(Nt)$. The best and second-best positions are then updated in $O(N)$. Several scalar control parameters are computed once per iteration in $O(1)$ or $O(N)$ for vectorized factors like Aroma-trajectory, Levy, and others, with combined cost $O(N)$.

Subsequently, for each of the N agents, a sequence of operations is performed, including random sampling, distance calculations, arithmetic operations on d-dimensional vectors, and several conditional behaviors. Each agent update involves $O(d)$ operations for position updates and distance calculations, while the control parameter and scalar factor updates remain in $O(1)$. Therefore, the total cost per iteration for agent updates is $O(Nd)$.

Multiplying by the number of iterations gives the overall optimization phase complexity as $O(T \times (Nd + Nt))$. If each fitness evaluation involves processing m samples over d features, the total time complexity of the algorithm becomes: $O(T \times N \times (md + d)) = O(T \times N \times md)$. As the md term dominates. Hence, the algorithm scales linearly with the number of agents, iterations, features, and data samples per evaluation.

TABLE II. PERFORMANCE COMPARISON RESULTS FOR CEC2022 BENCHMARK FUNCTION OPTIMIZATION

Function		CPO	ICPO1	ICPO2	ICPO3	ICPO4	ICPO5	ICPO6
F1	Ave	3.8914E+04	1.9154E+04	1.8045E+04	2.3228E+04	**1.5692E+04**	1.8903E+04	2.0389E+04
	Std	1.0692E+04	9.7637E+03	9.7121E+03	1.3325E+04	**6.0022E+03**	1.0527E+04	9.4372E+03
	Best	2.3743E+04	7.8363E+03	4.6172E+03	6.7316E+03	9.1717E+03	**6.1090E+03**	9.1516E+03
	Rank	7	4	2	6	1	3	5
F2	Ave	4.6777E+02	4.5664E+02	4.5969E+02	**4.5305E+02**	4.5941E+02	4.5465E+02	4.5788E+02
	Std	1.8486E+01	**1.0740E+01**	1.2275E+01	1.5503E+01	1.1463E+01	1.3732E+01	1.7308E+01
	Best	4.4927E+02	4.4529E+02	4.4686E+02	**4.0341E+02**	4.4534E+02	4.2212E+02	4.0438E+02
	Rank	7	3	6	1	5	2	4
F3	Ave	6.6500E+02	**6.4199E+02**	6.4591E+02	6.5249E+02	6.4337E+02	6.4476E+02	6.5436E+02
	Std	8.8120E+00	2.0538E+01	1.7990E+01	1.9964E+01	**1.4190E+01**	1.6649E+01	2.1810E+01
	Best	6.4758E+02	**6.1327E+02**	6.2295E+02	6.2574E+02	6.2458E+02	6.2532E+02	6.1590E+02
	Rank	7	1	4	5	2	3	6
F4	Ave	8.9384E+02	8.8555E+02	8.8941E+02	8.8712E+02	**8.8130E+02**	9.0139E+02	8.8657E+02

F5	Std	6.0398E+00	2.3057E+01	2.4783E+01	6.1075E+00	2.1503E+01	3.6264E+01	**1.4267E+01**
	Best	8.7998E+02	8.4510E+02	8.5753E+02	8.7767E+02	8.3847E+02	8.4099E+02	**8.3071E+02**
	Rank	6	2	5	4	1	7	3
F6	Ave	3.5628E+03	3.0554E+03	3.0509E+03	3.2955E+03	3.0699E+03	3.2250E+03	**2.6756E+03**
	Std	6.0031E+02	8.9616E+02	7.6217E+02	7.0222E+02	8.2390E+02	**5.1505E+02**	1.0271E+03
	Best	2.5623E+03	1.3662E+03	1.1472E+03	1.7762E+03	1.1089E+03	2.1223E+03	**9.2793E+02**
	Rank	7	3	2	6	4	5	1
	Ave	3.1337E+04	1.3655E+04	**8.0287E+03**	1.0419E+04	1.2247E+04	8.2018E+03	9.5090E+03
	Std	3.9863E+04	3.1619E+04	8.9712E+03	8.7805E+03	1.2997E+04	7.2484E+03	**6.8668E+03**
	Best	6.5577E+03	**2.0684E+03**	2.2470E+03	2.1061E+03	2.4944E+03	2.5591E+03	2.3653E+03
	Rank	7	6	1	4	5	2	3
F7	Ave	2.2933E+03	2.1693E+03	2.1462E+03	2.1659E+03	**2.1262E+03**	2.1458E+03	2.1927E+03
	Std	1.5487E+02	7.7798E+01	6.1200E+01	7.5971E+01	4.6186E+01	**3.9464E+01**	7.9594E+01
	Best	2.1251E+03	2.0740E+03	**2.0563E+03**	2.0980E+03	2.0670E+03	2.0765E+03	2.0807E+03
	Rank	7	5	3	4	1	2	6
F8	Ave	2.5012E+03	**2.3219E+03**	2.3376E+03	2.3268E+03	2.3363E+03	2.3264E+03	2.3621E+03
	Std	1.9316E+02	1.0330E+02	1.0147E+02	**9.7896E+01**	1.0737E+02	1.0797E+02	1.2988E+02
	Best	2.2311E+03	2.2303E+03	2.2260E+03	2.2315E+03	2.2282E+03	2.2294E+03	**2.2269E+03**
	Rank	7	1	5	3	4	2	6
F9	Ave	2.5197E+03	2.5120E+03	2.4918E+03	2.5061E+03	2.5072E+03	**2.4895E+03**	2.4942E+03
	Std	2.2205E+01	6.2304E+01	1.9353E+01	5.2791E+01	4.7704E+01	**7.0421E+00**	1.4606E+01
	Best	2.4869E+03	2.4821E+03	**2.4818E+03**	2.4828E+03	2.4825E+03	2.4837E+03	2.4827E+03
	Rank	7	6	2	4	5	1	3
F10	Ave	6.4695E+03	**2.7607E+03**	3.4674E+03	3.2271E+03	3.0439E+03	3.5046E+03	4.4277E+03
	Std	1.5014E+03	9.8732E+02	1.5402E+03	1.3633E+03	**1.2885E+03**	1.7241E+03	1.9854E+03
	Best	3.0178E+03	**2.5005E+03**	2.5006E+03	2.5005E+03	2.5007E+03	2.5005E+03	2.5006E+03
	Rank	7	1	4	3	2	5	6
F11	Ave	3.1153E+03	2.9757E+03	2.9519E+03	**2.9337E+03**	2.9356E+03	2.9729E+03	2.9637E+03
	Std	4.0457E+02	**3.2548E+01**	3.5021E+01	8.2107E+01	1.1296E+02	3.5319E+01	3.6715E+01
	Best	2.6030E+03	2.9178E+03	2.9202E+03	2.6206E+03	**2.6143E+03**	2.9223E+03	2.9212E+03
	Rank	7	6	3	1	2	5	4
F12	Ave	3.2874E+03	3.0964E+03	3.0759E+03	3.1019E+03	**3.0581E+03**	3.0817E+03	3.0699E+03
	Std	2.3245E+02	9.9663E+01	1.0314E+02	1.1913E+02	9.2301E+01	1.1145E+02	**6.0678E+01**
	Best	2.9947E+03	2.9761E+03	2.9570E+03	**2.9518E+03**	2.9631E+03	2.9656E+03	2.9602E+03
	Rank	7	5	3	6	1	4	2
Friedman Rank		6.92	3.58	3.33	3.92	2.75	3.42	4.08
Final Ranking		7	4	2	5	1	3	6

TABLE III. GENERATOR SET CHARACTERISTICS OF 40-UNIT

Unit	α_i	β_i	γ_i	P_{min}	P_{max}	e_i	f_i
1	94.705	6.73	0.0069	36	114	100	0.084
2	94.705	6.73	0.0069	36	114	100	0.084
3	309.54	7.07	0.02028	60	120	100	0.084
4	369.03	8.18	0.00942	80	190	150	0.063
5	148.89	5.35	0.0114	47	97	120	0.077
6	222.33	8.05	0.01142	68	140	100	0.084
7	267.71	8.03	0.00357	110	300	200	0.042
8	391.98	6.99	0.00492	135	300	200	0.042
9	455.76	6.60	0.00573	135	300	200	0.042
10	722.82	12.9	0.00605	130	300	200	0.042
11	635.2	12.9	0.00515	94	375	200	0.042
12	654.69	12.8	0.00569	94	375	200	0.042

13	913.4	12.5	0.00421	125	500	300	0.035
14	1760.4	8.84	0.00752	125	500	300	0.035
15	1728.3	9.15	0.00708	125	500	300	0.035
16	1726.3	9.15	0.00708	125	500	300	0.035
17	647.85	7.97	0.00313	220	500	300	0.035
18	649.69	7.95	0.00313	220	500	300	0.035
19	647.83	7.97	0.00313	242	550	300	0.035
20	647.81	7.97	0.00313	242	550	300	0.035
21	785.96	6.63	0.00298	254	550	300	0.035
22	785.96	6.63	0.00298	254	550	300	0.035
23	794.53	6.66	0.00284	254	550	300	0.035
24	794.53	6.66	0.00284	254	550	3o0	0.035
25	801.32	7.10	0.00277	254	550	300	0.035
26	801.32	7.10	0.00277	254	550	300	0.035
27	1055.1	3.33	0.52124	10	150	120	0.077
28	1055.1	3.33	0.52124	10	150	120	0.077
29	1055.1	3.33	0.52124	10	150	120	0.077
30	148.89	5.35	0.01140	47	97	120	0.077
31	222.92	6.43	0.00160	60	190	150	0.063
32	222.92	6.43	0.00160	60	190	150	0.063
33	222.92	6.43	0.00160	60	190	150	0.063
34	107.87	8.95	0.0001	90	200	200	0.042
35	116.58	8.62	0.0001	90	200	200	0.042
36	116.58	8.62	0.0001	90	200	200	0.042
37	307.45	5.88	0.0161	25	110	80	0.098
38	307.45	5.88	0.0161	25	110	80	0.098
39	307.45	5.88	0.0161	25	110	80	0.098
40	647.83	7.97	0.00313	242	550	300	0.035

TABLE IV. THE OPTIMAL SOLUTION VALUES FOR THE FUEL COST OF THE 40-UNIT SYSTEM

	ICPO	WOA	COA	HHO	ZOA	AOA
P_1	113.94	114	93.72	85.69	114	114
P_2	113.38	48.31	95.85	93.14	114	114
P_3	115.03	108.93	64.72	112.76	120	115.64
P_4	188.77	103.91	169.25	176.76	190	190
P_5	96.99	97	87.72	95.33	97	97
P_6	139.73	91.25	139.54	135.10	123.64	113.59
P_7	297.51	282.99	259.68	266.86	300	254.86
P_8	299.74	243.79	286.73	297.17	300	300
P_9	198.34	300	251.78	287.09	300	300
P_{10}	140.68	300	180.18	279.56	194.39	300
P_{11}	208.36	375	192.43	232.44	172.42	323.38
P_{12}	152.76	317.39	372.14	229.90	106.75	145.62
P_{13}	233.48	295.52	482.86	310.26	427.05	252.87
P_{14}	317.76	340.97	475.37	307.99	197.95	431.21
P_{15}	298.43	167.74	492.45	314.34	500	277.69
P_{16}	467.01	500	259.31	312.95	478.29	155.72
P_{17}	380.45	500	490.03	467.73	500	482.58
P_{18}	447.93	500	453.68	471.06	220	455.17
P_{19}	516.49	337.42	348.66	518.02	550	550
P_{20}	508.90	550	330.70	515.74	550	550
P_{21}	548.25	482.44	478.97	517.92	525.70	461.47

P_{22}	521.95	550	548.61	503.95	550	550
P_{23}	543.13	550	320.50	520.48	550	550
P_{24}	506.32	550	478.93	525.06	334.68	461.47
P_{25}	543.46	387.95	520.96	523.43	550	461.47
P_{26}	522.94	520.68	473.01	518.82	550	550
P_{27}	10.20	35.91	20.83	33.26	23.37	30.30
P_{28}	10.31	17.03	16.12	21.59	37.63	27.60
P_{29}	10.32	33.27	135.61	27.01	10	55.15
P_{30}	95.87	97	96.24	88.68	97	58.28
P_{31}	189.97	81.57	150.59	153.06	60	190
P_{32}	189.89	78.69	177.82	154.29	190	162.48
P_{33}	189.82	136.38	163.13	144.78	132.74	190
P_{34}	199.47	200	193.01	189.60	200	129.12
P_{35}	199.93	200	116.93	191.58	200	200
P_{36}	197.41	200	189.30	190.11	135.33	192.98
P_{37}	98.39	110	108.23	63.28	110	95.14
P_{38}	105.88	34.85	108.55	61.47	110	110
P_{39}	109.68	110	102.53	70.84	33.14	95.14
P_{40}	471.14	550	548.55	490.88	550	403.69
P_D	1.05E+04	1.05E+04	1.05E+04	1.05E+04	1.05E+04	1.05E+04
Fuel Cost($)	121336.92	131459.60	130208.16	123727.97	125700.53	123036.11

TABLE V. GENERATOR SET CHARACTERISTICS OF 110-UNIT

Unit	α_i	β_i	γ_i	P_{min}	P_{max}	Unit	α_i	β_i	γ_i	P_{min}	P_{max}
1	12	2.4	0.0253	25.547	24.389	56	96	25.2	0.0098	14.327	82.136
2	12	2.4	0.0265	25.675	24.411	57	96	25.2	0.0099	14.354	82.298
3	12	2.4	0.028	25.803	24.638	58	100	35	0.0092	14.38	82.464
4	12	2.4	0.0284	25.932	24.76	59	100	35	0.0094	14.407	82.626
5	12	2.4	0.0286	26.061	24.888	60	120	45	0.0072	19	218.895
6	20	4	0.0120	37.551	117.755	61	120	45	0.0071	19.1	219.335
7	20	4	0.0126	37.664	118.108	62	120	45	0.007	19.2	219.775
8	20	4	0.0136	37.777	118.458	63	185	54.3	0.0066	11.694	143.735
9	20	4	0.0143	37.89	118.821	64	185	54.3	0.0057	11.715	144.029
10	76	15.2	0.0088	13.327	81.136	65	185	54.3	0.0058	11.737	144.318
11	76	15.2	0.0089	13.354	81.298	66	185	54.3	0.0059	11.758	144.597
12	76	15.2	0.0091	13.8	81.464	67	197	70	0.0036	24	269.131
13	76	15.2	0.0093	13.407	81.626	68	197	70	0.0036	24.1	269.649
14	100	25	0.0062	18	217.895	69	197	70	0.0036	24.2	270.176
15	100	25	0.0061	18.1	218.335	70	360	150	0.0025	11.862	187.057
16	100	25	0.006	18.2	218.775	71	400	160	0.0029	8.492	320.002
17	155	54.3	0.0046	10.694	142.735	72	400	160	0.003	8.503	321.91
18	155	54.3	0.0047	10.715	143.029	73	300	60	0.0054	13.327	52.136
19	155	54.3	0.0048	10.737	143.318	74	250	50	0.0055	12.354	42.298
20	155	54.3	0.0049	10.758	143.597	75	90	30	0.0099	11.38	32.464
21	197	68.9	0.0026	23	259.131	76	50	12	0.0031	9.407	23.626
22	197	68.9	0.0026	23.1	259.649	77	450	160	0.0024	14	220
23	197	68.9	0.0026	23.2	260.176	78	600	150	0.0023	13.1	190
24	350	140	0.0015	10.862	177.057	79	200	50	0.0036	13.2	250
25	400	100	0.0019	7.492	210.002	80	120	20	0.0049	13.5	230
26	400	100	0.0019	7.503	211.91	81	55	10	0.0061	24	70
27	500	140	0.0014	12	210	82	40	12	0.007	14.5	60
28	500	140	0.0013	12.1	180	83	80	20	0.0088	14.2	210

29	200	50	0.0026	12.2	240	84	200	50	0.0022	13.4	150
30	100	25	0.0039	12.5	220	85	325	80	0.0048	11.3	130
31	50	10	0.0051	23	60	86	440	120	0.0053	8.9	80
32	20	5	0.005	13.5	50	87	35	10	0.0021	14.4	90
33	80	20	0.0078	13.2	200	88	55	20	0.0033	14.3	80
34	250	75	0.0012	12.4	140	89	100	20	0.0034	13.9	125
35	360	110	0.0038	10.3	120	90	220	40	0.0037	13.8	160
36	400	130	0.0043	9.9	90	91	140	30	0.0066	13.7	50
37	40	10	0.0011	13.4	80	92	100	40	0.0043	13.6	400
38	70	20	0.0023	13.3	70	93	440	100	0.0022	8.4	260
39	100	25	0.0034	12.9	115	94	500	100	0.0055	7.6	110
40	120	20	0.0067	12.8	150	95	600	100	0.0032	7.5	170
41	180	40	0.0056	12.7	40	96	700	200	0.0077	7.2	140
42	220	50	0.0023	12.6	300	97	15	3.6	0.0353	26.547	26.389
43	440	120	0.0012	7.4	250	98	15	3.6	0.0365	26.675	25.411
44	560	160	0.0045	6.6	100	99	22	4.4	0.038	26.803	25.638
45	660	150	0.0022	6.5	160	100	22	4.4	0.0384	26.932	25.76
46	700	200	0.0067	6.2	130	101	60	10	0.021	15.3	65
47	32	5.4	0.0353	26.547	34.389	102	80	10	0.023	16	82
48	32	5.4	0.0365	26.675	34.411	103	100	20	0.024	20.2	86
49	52	8.4	0.038	26.803	34.638	104	120	20	0.035	20.2	84
50	52	8.4	0.0384	26.932	34.761	105	150	40	0.034	25.6	75
51	52	8.4	0.0386	17.061	34.888	106	280	40	0.037	30.5	56
52	60	12	0.032	38.551	127.755	107	520	50	0.039	32.5	67
53	60	12	0.0326	36.664	128.108	108	150	30	0.035	26	68
54	60	12	0.0236	38.777	128.458	109	320	40	0.028	25.8	69
55	60	12	0.0243	38.89	128.821	110	200	20	0.026	27	72

TABLE VI. THE OPTIMAL SOLUTION VALUES FOR THE FUEL COST OF THE 110-UNIT SYSTEM

Algorithm	ICPO	WOA	COA	HHO	POA	AOA
P_1	11.15	4.93	10.98	6.91	5.75	2.4
P_2	5.11	11.57	2.52	6.72	2.40	2.4
P_3	4.46	5.28	12	7.69	5.77	2.4
P_4	2.57	3.37	12	5.16	4.11	12
P_5	8.22	11.64	12	9.64	4.34	12
P_6	5.12	6.65	20	7.46	20	4
P_7	4.02	7.53	20	10.87	14.92	20
P_8	8.96	7.68	20	20.00	5.72	20
P_9	16.01	18.86	20	14.98	15.75	4
P_{10}	69.96	46.58	76	42.14	76	76
P_{11}	69.79	73.90	76	60.45	15.2	76
P_{12}	71.20	26.05	41.15	66.99	31.33	15.2
P_{13}	18.11	67.78	76	38.50	43.23	76
P_{14}	25.75	99.75	25.13	40.62	65.34	100
P_{15}	35.46	54.10	72.47	99.35	67.36	100
P_{16}	63.05	31.47	25	46.02	100	100
P_{17}	151.88	148.57	78.93	65.97	153.77	54.3
P_{18}	149.68	92.44	155	138.80	73.92	155
P_{19}	140.80	94.66	155	77.51	145.51	155
P_{20}	154.42	153.80	155	105.88	125.02	155
P_{21}	167.68	117.04	93.83	86.40	152.85	197
P_{22}	116.46	144.45	119.42	93.14	68.9	68.9

P_{23}	149.14	189.93	197	181.04	117.37	68.9
P_{24}	252.76	349.15	350	269.51	253.84	140
P_{25}	310.27	273.87	134.86	372.34	263.01	120.14
P_{26}	355.08	207.20	215.72	239.52	400	400
P_{27}	481.35	326.74	226.14	499.95	500	500
P_{28}	476.81	278.94	373.71	450.55	361.02	192.25
P_{29}	142.82	123.14	200	68.18	94.77	50
P_{30}	94.20	93.69	100	99.99	95.99	100
P_{31}	17.81	14.81	50	18.26	45.74	10
P_{32}	19.03	12.08	17.37	11.22	5	5
P_{33}	64.98	39.12	44.42	25.10	70.91	20
P_{34}	212.52	221.83	250	172.00	250	250
P_{35}	323.76	257.00	360	260.12	185.40	360
P_{36}	233.54	357.76	271.89	376.34	400	130
P_{37}	27.94	14.92	32.17	22.92	33.28	40
P_{38}	58.08	24.11	20	53.55	20	70
P_{39}	99.60	84.43	100	41.22	92.35	25
P_{40}	101.14	87.21	120	119.99	21.70	20
P_{41}	141.50	79.81	180	127.02	51.60	40
P_{42}	215.69	106.38	51.12	142.14	99.38	220
P_{43}	433.45	397.54	440	439.96	272.99	440
P_{44}	466.84	409.42	560	527.55	560	560
P_{45}	619.30	531.64	660	640.51	660	660
P_{46}	540.41	577.09	700	452.63	700	700
P_{47}	24.35	14.44	32	13.36	9.34	32
P_{48}	10.63	8.27	22.25	25.39	5.4	32
P_{49}	9.28	12.85	52	30.40	52	52
P_{50}	18.69	51.67	52	27.87	8.4	52
P_{51}	10.51	44.66	42.45	21.77	29.34	52
P_{52}	12.58	53.76	29.86	59.22	51.75	60
P_{53}	14.92	29.82	60	43.38	24.78	60
P_{54}	12.16	15.85	56.71	42.84	13.94	60
P_{55}	15.73	35.07	29.84	21.84	36.50	12
P_{56}	84.95	83.57	96	88.45	80.53	96
P_{57}	76.32	47.33	96	80.89	37.58	96
P_{58}	40.72	58.33	100	96.78	94.20	100
P_{59}	56.37	98.98	100	72.59	73.82	100
P_{60}	50.30	118.33	54.70	84.10	77.78	120
P_{61}	56.23	72.63	77.87	115.67	115.73	45
P_{62}	45.74	106.64	45	67.88	76.15	45
P_{63}	171.93	71.42	185	155.92	119.53	54.3
P_{64}	184.00	137.35	185	77.61	151.12	54.3
P_{65}	167.79	114.36	75.12	184.98	142.99	185
P_{66}	185	86.35	131.76	164.31	89.27	185
P_{67}	93.45	124.79	156.46	107.25	197	197
P_{68}	89.66	196.21	70	172.45	96.09	197
P_{69}	108.86	194.19	70	196.98	197	197
P_{70}	334.06	342.69	360	248.29	360	150
P_{71}	266.14	378.21	400	190.92	387.76	400
P_{72}	381.47	240.72	201.64	240.58	400	400
P_{73}	86.12	148.42	300	143.21	185.13	300
P_{74}	158.30	192.75	250	141.57	121.92	250

P_{75}	84.43	88.00	90	89.99	34.15	30
P_{76}	49.73	13.76	42.66	16.84	24.71	50
P_{77}	359.56	361.53	208.53	449.97	377.29	450
P_{78}	334.17	491.20	407.95	400.78	600	270.33
P_{79}	195.63	166.39	167.51	144.75	50	200
P_{80}	89.08	115.11	120	45.93	29.63	20
P_{81}	12.91	42.68	55	54.99	15.94	10
P_{82}	34.98	17.65	40	25.32	31.82	40
P_{83}	30.97	45.56	80	68.62	21.74	20
P_{84}	184.07	167.57	70.87	87.21	125.50	200
P_{85}	252.59	320.84	325	269.11	325	325
P_{86}	381.41	150.14	290.52	439.96	227.63	440
P_{87}	24.20	34.69	35	32.77	31.12	35
P_{88}	39.70	49.23	20	29.14	36.58	55
P_{89}	89.06	88.06	100	70.08	21.26	20
P_{90}	165.94	101.29	116.13	219.98	40	40
P_{91}	74.03	90.51	30	120.91	99.51	30
P_{92}	99.81	70.04	40	63.82	75.84	40
P_{93}	200.95	413.80	440	245.57	414.11	440
P_{94}	496.96	410.74	216.43	346.32	500	180.19
P_{95}	580.55	508.48	382.82	415.13	600	600
P_{96}	394.39	579.68	700	627.54	276.96	700
P_{97}	10.79	6.95	15	10.65	14.13	3.6
P_{98}	13.55	14.94	3.6	9.84	11.65	14.99
P_{99}	4.94	8.35	8.73	13.90	15.97	22
P_{100}	7.33	15.69	13.59	15.58	16.02	22
P_{101}	10.20	21.38	10.86	40.87	37.53	60
P_{102}	16.08	78.39	80	42.85	69.86	10
P_{103}	38.23	37.61	50.41	99.99	20	100
P_{104}	20.66	89.04	120	91.71	97.88	120
P_{105}	122.37	96.91	94.87	132.23	40.34	40
P_{106}	110.11	132.58	40	202.99	280	40
P_{107}	263.58	383.77	50	263.59	113.96	50
P_{108}	87.79	100.45	30	46.32	98.98	150
P_{109}	117.59	156.05	40	95.62	45.02	40
P_{110}	97.49	165.42	200	89.76	188.40	20
P_D	1.50E+04	1.50E+04	1.50E+04	1.50E+04	1.50E+04	1.50E+04
Fuel Cost($/h)	221621.01	241792.64	224933.39	236963.17	231688.22	228383.93

VI. Conclusion

This paper introduces an enhanced Chinese Pangolin Optimizer (CPO), incorporating a probability oscillation convergence factor strategy to address the Economic Load Dispatch (ELD) problem. The proposed method boosts the algorithm's global search capacity and local exploration efficiency by incorporating six distinct probability distributions: uniform, Beta, exponential, normal, Rayleigh and Weibull distributions. This diverse approach significantly improves the optimization accuracy and solution stability by providing varied search dynamics and adaptability to different problem landscapes.

To assess the effectiveness of the proposed method, comprehensive experiments were initially conducted using the CEC-BC-2022 benchmark functions to evaluate the optimization performance of the enhanced CPO algorithm. Based on these findings, the most effective strategy for addressing the Economic Load Dispatch (ELD) problem was determined. Subsequently, the algorithm was tested under two distinct power system configurations: the first scenario involved 40 generators with a total power demand of 10,500 MW, and the second involved 110 generators with a total demand of 15,000 MW. The results demonstrate that the improved CPO algorithm outperforms traditional optimization methods in terms of reducing fuel costs, minimizing power losses, and achieving faster convergence.

These outcomes underscore the algorithm's robustness and adaptability, positioning it as a highly promising solution for practical ELD problems.

This advancement offers an efficient and reliable intelligent optimization tool for power system operators, facilitating the reduction of operational costs and enhancing the economic performance of power grids. Moreover, the proposed CPO algorithm can serve as a foundation for the development of more sophisticated optimization techniques in the power system domain.

Future research could explore the incorporation of more dynamic and adaptive convergence factor strategies, potentially in conjunction with advanced techniques such as deep learning or reinforcement learning. Such integration would enhance the algorithm's capability to tackle complex constraints and large-scale optimization problems, broadening its applicability to more complex and diverse power system optimization scenarios. Additionally, these advancements could improve the algorithm's performance in dynamic, real-time system environments, thereby increasing its potential for practical deployment in the energy sector.

REFERENCES

[1] H. A. de Sá Leitão, P. A. C. Rosas, and G. L. M. Júnior. "Economic Load Dispatch in Brazilian Isolated Electricity System: A Case Study of Oiapoque," *Renewable Energy*, vol. 245, pp. 122695, 2025.

[2] A. Sabo, S. Buba, and K. Muhammed. "A Review on Techniques Used for Solving the Economic Load Dispatch Problems: Categorization, Advantages, and Limitations," *Vokasi Unesa Bulletin of Engineering, Technology and Applied Science*, vol. 2, no. 1, pp. 36-47, 2025.

[3] S. Si-Ma, H. M. Liu, and H. X. Zhan. "Efficient Maximum Iterations for Swarm Intelligence Algorithms: A Comparative Study," *Artificial Intelligence Review*, vol. 58, no. 3, pp. 87, 2025.

[4] N. K. Yadav. "Hybridization of Differential Evolution and Particle Swarm Optimization with Distributed Acceleration Constants to Solve Economic Load Dispatch Problem," *Applied Intelligence*, vol. 55, no. 5, pp. 332, 2025.

[5] M. H. Hassan, S. Kamel, and F. Jurado. "Global Optimization of Economic Load Dispatch in Large Scale Power Systems Using an Enhanced Social Network Search Algorithm," *International Journal of Electrical Power & Energy Systems*, vol. 156, pp. 109719, 2024.

[6] A. Srivastava and D. K. Das. "A New Aggrandized Class Topper Optimization Algorithm to Solve Economic Load Dispatch Problem in a Power System," *IEEE Transactions on Cybernetics*, vol. 52, no. 6, pp. 4187-4197, 2020.

[7] W. K. Hao, J. S. Wang, and X. D. Li. "Arithmetic Optimization Algorithm Based on Elementary Function Disturbance for Solving Economic Load Dispatch Problem in Power System," *Applied Intelligence*, vol. 52, no. 10, pp. 11846-11872, 2022.

[8] M. A. Al-Betar, M. A. Awadallah, and M. M. Krishan. "A Non-Convex Economic Load Dispatch Problem with Valve Loading Effect Using a Hybrid Grey Wolf Optimizer," *Neural Computing and Applications*, vol. 32, no. 16, pp. 12127-12154, 2020.

[9] T. Singh. "Chaotic Slime Mould Algorithm for Economic Load Dispatch Problems," *Applied Intelligence*, vol. 52, no. 13, pp. 15325-15344, 2022.

[10] Y. Zhang, and H. Li. "Research on Economic Load Dispatch Problem of Microgrid Based on an Improved Pelican Optimization Algorithm," *Biomimetics*, vol. 9, no. 5, pp. 277, 2024.

[11] J. S. Pan, J. Shan, and S. C. Chu. "A Multigroup Marine Predator Algorithm and Its Application for the Power System Economic Load Dispatch," *Energy Science & Engineering*, vol. 10, no. 6, pp. 1840-1854, 2022.

[12] K. Yang and K. Yang. "Improved Whale Algorithm for Economic Load Dispatch Problem in Hydropower Plants and Comprehensive Performance Evaluation," *Water Resources Management*, vol. 36, no. 15, pp. 5823-5838, 2022.

[13] M. H. Hassan, S. Kamel, and A. Selim. "Efficient Economic Operation Based on Load Dispatch of Power Systems Using a Leader White Shark Optimization Algorithm," *Neural Computing and Applications*, vol. 36, no. 18, pp. 10613-10635, 2024.

[14] Z. Guo, G. Liu, and F. Jiang. "Chinese Pangolin Optimizer: A Novel Bio-Inspired Metaheuristic for Solving Optimization Problems," *The Journal of Supercomputing*, vol. 81, no. 4, pp. 517, 2025.

[15] S. Patty, R. Das, and D. Mandal. "Self-Adaptive Multi-Population Quadratic Approximation Guided Jaya Optimization Applied to Economic Load Dispatch Problems With or Without Valve-Point Effects," *Results in Control and Optimization*, pp. 100543, 2025.

[16] J. Zhang, H. Li, and M. K. Parizi. "HWMWOA: A Hybrid WMA-WOA Algorithm with Adaptive Cauchy Mutation for Global Optimization and Data Classification," *International Journal of Information Technology & Decision Making*, vol. 22, no. 4, pp. 1195-1252, 2023.

[17] S. T. Shishavan, and F. S. Gharehchopogh. "An Improved Cuckoo Search Optimization Algorithm with Genetic Algorithm for Community Detection in Complex Networks," *Multimedia Tools and Applications*, vol. 81, no. 18, pp. 25205-25231, 2022.

[18] B. K. Tripathy, P. K. Reddy Maddikunta, and Q. V. Pham. "Harris Hawk Optimization: A Survey on Variants and Applications," *Computational Intelligence and Neuroscience*, vol. 2022, no. 1, pp. 2218594, 2022.

[19] P. Trojovský and M. Dehghani. "Pelican Optimization Algorithm: A Novel Nature-Inspired Algorithm for Engineering Applications," *Sensors*, vol. 22, no. 3, pp. 855, 2022.

[20] L. Abualigah, A. Diabat, and S. Mirjalili. "The Arithmetic Optimization Algorithm," *Computer Methods in Applied Mechanics and Engineering*, vol. 376, pp. 113609, 2021.